Nuclear Instruments and Methods in Physics Research A 740 (2014) 6–9

Contents lists available at ScienceDirect

Nuclear Instruments and Methods in Physics Research A

journal homepage: www.elsevier.com/locate/nima

Laser-driven ion acceleration: State of the art and emerging mechanisms

Marco Borghesi [a,b,*]

[a] Centre for Plasma Physics, The Queen's University of Belfast, Belfast BT7 1NN, United Kingdom
[b] Institute of Physics of the ASCR, ELI-Beamlines Project, Na Slovance 2, 18221 Prague, Czech Republic

ARTICLE INFO

Available online 26 December 2013

Keywords:
Laser acceleration of ions
Sheath acceleration
Radiation pressure
Laser-matter nteraction

ABSTRACT

Ion acceleration driven by high intensity laser pulses is attracting an impressive and steadily increasing research effort. Experiments over the past 10–15 years have demonstrated, over a wide range of laser and target parameters, the generation of multi-MeV proton and ion beams with unique properties, which have stimulated interest in a number of innovative applications. While most of this work has been based on sheath acceleration processes, where space-charge fields are established by relativistic electrons at surfaces of the irradiated target, a number of novel mechanisms has been the focus of recent theoretical and experimental activities. This paper will provide a brief review of the state of the art in the field of laser-driven ion acceleration, with particular attention to recent developments.

1. Introduction

The first experiments reporting laser acceleration of protons with beam-like properties and multi-MeV energies in laser experiments were reported in 2000 [1–3]. Experiments over the following 13 years have demonstrated, over a wide range of laser and target parameters, the generation of multi-MeV proton and ion beams with unique properties such as ultrashort burst emission, high brilliance, and low emittance, which have in turn stimulated ideas for a range of innovative applications. While most of this work has been based on sheath acceleration processes [3–5], a number of novel mechanisms have been at the center of recent theoretical and experimental activities. This paper will provide a brief review of the state of the art and recent developments in the field. A more extensive survey is provided in [6–8].

2. Sheath acceleration

This is the acceleration mechanism active in most experiments carried out so far, and it was proposed [4] as an interpretative framework of the multi-MeV proton observations reported in [2], obtained on the NOVA Petawatt laser at LLNL (the name *Target Normal Sheath Acceleration*, TNSA, is generally used).

Acceleration through this mechanism employs thin foils (typically from a few μm to tens of μm thickness), which are irradiated by an intense laser pulse. In the intensity regime of relevance (as a guideline, $I\lambda^2 > 10^{18}$ W/cm^2), the laser pulse can couple efficiently energy into relativistic electrons, mainly through ponderomotive processes (e.g., $J \times B$ mechanism [9]). The average energy of the electrons is typically of MeV order, e.g., their collisional range is much larger than the foil thickness, so that they can propagate to the rear of the target, and drive the acceleration of ions from surface layers via the space-charge field established as they try to move away from the target. While a limited number of energetic electrons will effectively leave the target, most of the hot electrons will be backheld within the target volume by the space charge, and will form a sheath extending by approximately a Debye length λ_D from the initially unperturbed rear surface. According to the model developed in [2], the initial accelerating field will be given by

$$E(0) = \frac{KT_h}{e\lambda_D} = \sqrt{\frac{n_h KT_h}{e\lambda_D}} \quad (1)$$

where n_h and T_h are density and temperature of the hot electrons, which for typical values at $I\lambda^2 \sim 10^{19}$ W/cm^2, i.e., $\lambda_d \sim 1$ μm and $T_h \sim 1$ MeV, gives field amplitudes of order TV/m. Under the right combination of target thickness and pulse duration, the hot electrons recirculate through the target during the ion acceleration process, which can lead to an enhancement of the ion energy [10]. TNSA from the front surface has normally reduced efficiency due to the presence of a preplasma, although symmetric acceleration from front and rear has indeed been observed in ultra-high contrast interactions with moderate intensity ultrashort pulses, where front preplasma formation is effectively suppressed [11].

While TNSA can in principle accelerate any ion species present in surface layers, in most experimental settings this results in preferential acceleration of light ions (protons, carbon and oxygen ions) from

* Corresponding author at: Department of Physics and Astronomy, The Queen's University of Belfast, Belfast BT7 1NN, United Kingdom.
E-mail address: m.borghesi@qub.ac.uk

0168-9002/$ - see front matter © 2014 Elsevier B.V. All rights reserved.
http://dx.doi.org/10.1016/j.nima.2013.11.098

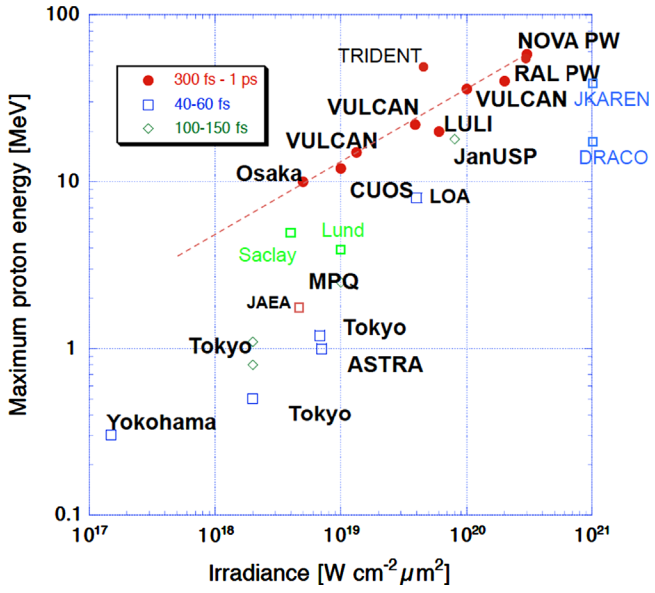

Fig. 1. Survey of TNSA cut-off energies measured in experiments so far, plotted vs. irradiance and labeled according to pulse duration. For references for the specific data points, see Refs. [6] and [13]. Points labeled J-Karen, DRACO and Trident refer respectively to Refs. [14–16].

contaminant layers rather than ions from the target bulk. Protons, with the highest charge to mass ratio, are therefore the dominant component of TNSA ion beams, unless the target is suitably treated prior to the laser irradiation to remove the contaminants [12].

According to (1) the field can be large enough to accelerate ions to multi-MeV energies, which have indeed been observed in a very large number of experiments. The energy spectra of the ion beams observed are broadband, typically with an exponential profile, up to a high energy cut-off, which is the quantity normally used to compare different experiments and determine experimental scaling laws for the acceleration process. The highest TNSA energies reported are of the order of 60 MeV, obtained with large PW systems, and available data (e.g., see Fig. 1) generally shows that, at equal intensities, longer pulses (of ~ps duration) containing more energy generally accelerate ions more efficiently than pulses with duration of tens of fs. Using state of the art fs systems has however recently allowed increasing the energies of accelerated protons up to a reported 40 MeV [14], obtained with only a few *J* of laser energy on target (see [17] for an up to date survey).

The properties of the beams accelerated via TNSA are quite different from those of conventional RF beams, to which they are superior under several aspects. The beams are characterized by ultralow transverse emittance (as low as 0.004 mm-mrad, according to the estimate given in [18]), and by ultrashort (~ps) duration at the source. The beams are bright, with 10^{11}–10^{13} protons per shot with energies > MeV, corresponding to currents in the kA range if co-moving electrons are removed. However, the number of protons at the high-energy end of the spectrum (i.e., the energies plotted in Fig. 1) can be as low as 10^{7}–10^{8} particles/MeV/sr, (e.g., see [17] for a discussion related to recently published data)- with a divergence of a few degrees this gives ~10^{6}–10^{7} particles/MeV. Drawbacks, as compared with conventional accelerator beams, are the larger divergence (up to 10 s of degrees, and energy dependent) and, as mentioned earlier, the broad spectrum.

3. Applications

A broad range of applications employing these ion beams has been proposed [8], some of which have been already implemented and use advantageously peculiar properties of the beams such as the extreme laminarity and short duration. Laser-driven proton radiography has allowed to map electric and magnetic fields in plasmas with very high spatial and temporal resolution, while exploiting the broad energy spectrum to achieve a multiframe capability [8]. The short duration of the ion bursts, coupled to their high flux, also facilitates the production of warm dense matter (i.e., matter at solid density and 1–100 eV temperatures) from isochorically heated samples [8]. In view of possible future use of laser-driven beams as a source for cancer radiotherapy, a number of experiments have investigated their biological effects on cellular media [8], reporting on-cell dose rates of the order of 10^{9} Gy/s [19,20], which are 9 orders of magnitude higher than normally used in radiobiology.

Future use of the beams in cancer therapy however, requires a marked improvement of the beam parameters currently available, as energies in the range of 150–300 MeV/nucleon are needed for treating deep-seated tumors with protons or carbon ions. A clinical fraction is currently delivered at 2–5 Gy/minutes, which, using 200 MeV on a typical tumor size ($5\times5\times5$ cm^3), requires the delivery of ~5×10^{8} particle per second. Other proposed applications in energy production schemes or schemes or particle physics also demand a significant progress. This motivates ongoing research aimed to improving the beam characteristics, either by optimizing TNSA acceleration or by exploring different mechanisms.

4. TNSA scaling and optimization

Increasing the laser intensity on target should generally lead to an increase of the cut-off energies of TNSA spectra, as shown in Fig. 1. However there is still debate on what is the most appropriate scaling for ion energies as a function of irradiance, and is also clear that, in addition to the role of pulse energy highlighted in Fig. 1, several secondary factors (e.g., such as prepulse energy and duration, target thickness) also affect the maximum energy measurable. Parametric investigations of the dependence of E_{max} on laser pulse irradiance, duration, energy and fluence have been reported (e.g., [15,16,21,22]). Two main classes of approaches have been developed to describe analytically the TNSA process with the aim of matching current results and predict performance at higher intensities. A first approach considers ions and hot electrons as an expanding plasma, described with fluid models [4,5,21] as an extension of the classical case of a plasma expanding into vacuum, driven by the ambipolar electric field generated in a narrow layer at the front of the plasma cloud. Simplest models are isothermal, and require that the acceleration time is artificially constrained [22], while more realistic adiabatic models, accounting for the finite energy of the hot electrons, have also been developed [22,23].

A different class of models assumes that the most energetic ions are accelerated as test particles in a *static* sheath field, unperturbed by their acceleration. These *static* models rely on an accurate description of the sheath field based on realistic assumptions on the fast electron distributions. For example, in [24], a spatial truncation of the electric potential in the sheath is introduced, and used to develop a model for the maximum ion energy as a function of the relevant laser parameters (energy and intensity). Scalings for the ion energy based on this model appear to match a large fraction of experimental results so far [25], and can be used as a predictive tool for future performance. Taking 200 MeV H^{+} energy as a benchmark, predictions of the intensity requirement for reaching this cut-off value based on the two different approaches discussed above give intensities of mid 10^{21} W/cm^2 for ~ps pulses [22], and ~10^{22} W/cm^2 for 10 s of fs pulses [25].

Several approaches have been developed to improve TNSA efficiency by acting on the characteristics of the hot electron population driving the acceleration through modifications of the target design [8]. According to Ref. (1) the accelerating field can be modified either by increasing the electron density or the temperature. The use of the so-called *mass limited targets*, aims to reduce the transverse size of the accelerating foils and concentrating the electrons within a smaller volume so that their density is increased during the acceleration process. This approach was first demonstrated in Ref. [26] where reduction of the transverse size of the foil down to $20\times 20\ \mu m^2$ resulted in a 3-fold protons energy increase with respect to a large mm-size foil, jointly to a sizeable increase in conversion efficiency. The highest published TNSA proton energy so far (67.5 MeV) has been obtained by using specially designed targets, i.e., flat-top hollow micro-cones [27], based on a target design used in fast ignition experiments. In these targets the interaction of the laser pulse with the wall of the cones results in an increase of the number of fast electron at the high-energy end of the spectrum, and, consequently, an enhancement of the accelerating field. A further class of experiments aims to optimize laser energy absorption into hot electrons by structuring the target: a recent example of this approach is reported in Ref. [28], where foils coated with microspheres (diameter $\sim\lambda/2$) on the irradiated surface showed, compared to uncoated foils, a clear improvement in the energy cut-off of the spectrum of the accelerated protons. For a review of other approaches, including the use of foam layers, controlled pre-plasmas, or double pulses, see [8].

5. Emerging acceleration mechanisms

While experimental activity has focused until recently on the study of TNSA beams, other mechanisms have recently attracted a significant amount of theoretical and experimental attention, and some of these mechanisms are briefly discussed in the following sections. We refer the reader to Ref. [8] for a more thorough discussion.

5.1. Hole boring acceleration

The radiation pressure of an intense laser pulse can be coupled to the electrons of an overdense plasma slab via the ponderomotive force [31]

$$f_p = -\frac{m_e}{4}\frac{\partial}{\partial x}v_{os}^2(x)(1-\cos 2\omega_0 t) \quad (2)$$

where v_{os} is the quiver velocity of the electrons and ω_0 is the laser frequency.

The force has an oscillating term (which gives rise to $J\times B$ heating and creates a population of hot electrons [9]) and a steady term, which acts on the bulk of the electrons, and creates a space-charge field via their local displacement. If this is sustained for a long enough time, it can accelerate the target ions. In a semi-infinite target this leads to the so-called *Hole–Boring* (HB) phenomenon [29]. Ions are set in motion toward the interior of the target with the hole boring velocity, which is determined by the intensity of the laser and the density of the medium. The energy of the ions in this regime scales linearly with $I\rho^{-1}$ in a classical approach, although relativistic corrections (necessary at ultrahigh intensities) lead to a slower, more complex scaling [30].

In a recent experiment employing CO_2 lasers, evidence of "pure" monochromatic spectra originated from this type of mechanism has been observed [31]. This experiment employed gas jet targets, exploiting the fact that electron densities above $10^{19}\ cm^{-3}$ are already overdense for the $\sim 10\ \mu m$ wavelength of a CO_2 laser. The proton spectra obtained show a clean monoenergetic signal at ~ 1 MeV which is broadly consistent with HB in the conditions of the experiment. Although the energy observed so far through HB is modest, the dependence on both target density and laser intensity allows designing suitable acceleration scenarios for acceleration to hundreds of MeV, as suggested in [30,32] (see Fig. 2).

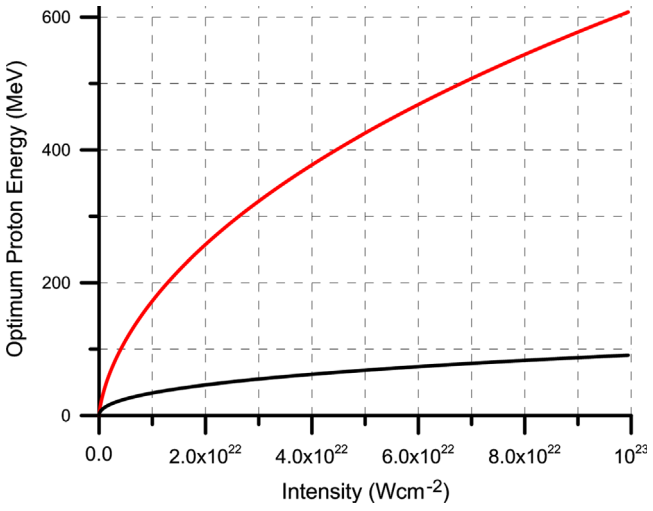

Fig. 2. Optimum proton energy obtainable from HB for a pure proton target as a function of intensity (from [32]) .The black line (slower trend) is a simple prediction based on opacity at the relativistically corrected critical density , the red line includes ponderomotive profile steepening. (For interpretation of the references to color in this figure legend, the reader is referred to the web version of this article.)

5.2. Shock acceleration

An acceleration scheme related to HB, but conceptually different, is the so-called *Shock Acceleration* (SA), first proposed in Ref. [33]. In this scheme, the light applied at the front surface of the target, acts as the source of a strong high Mach-number collisionless electrostatic shock propagating towards the bulk of the plasma. Acceleration arises as ions present in the bulk of the target are reflected from the shock front to twice the shock velocity. Recent results also obtained with a CO_2 laser have been explained with this mechanism, namely monoenergetic acceleration of protons up to 22 MeV from the interaction with hydrogen gas jets at intensities in the 10^{16}–$10^{17}\ W\ cm^2$ regime [34].

5.3. Light sail acceleration

The idea of applying ultraintense radiation pressure to a thin foil and drive forward the whole irradiated region of the foil under the effect of the laser piston was first proposed by Esirkepov et al. [35]. This concept was later developed by several other authors (e.g., [36,37]) and is now generally referred to as *Light Sail* (LS). In LS the irradiated region of an ultrathin foil is first compressed into a plasma slab through an initial HB phase, and then propelled forward in vacuum by the radiation pressure once the compressed layer has reached the rear of the foil [38,39].

LS is effective as long as the compressed foil stays opaque to the radiation, since target transparency implies a decrease of the radiation pressure drive [37]. Although the detailed dynamics are complex, in first approximation the overall motion of the foil can be modeled by assuming that the laser momentum is transferred to the thin foil [35], which leads to a fast scaling of the ion energy $\varepsilon\sim(I\tau\sigma^{-1})^2$ where $\sigma=\rho\tau$ is the foil's areal density (with t its thickness) [37] and implies natively narrow band spectra. For LS to be effective, it is essential that the radiation pressure is strong enough to overcome detrimental effects related to electron

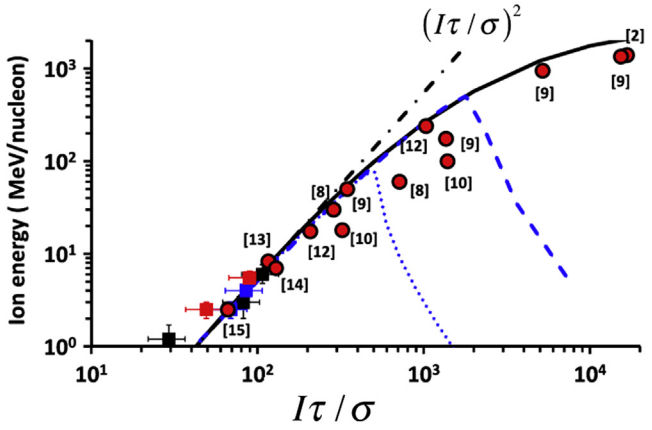

Fig. 3. LS energy scaling: experimental points (squares) and PIC predictions from literature (circles) are plotted against the simple $((I\tau\sigma^{-1})^2)$ scaling (dashed line) and a more extensive model including relativistic effects (solid line) (from [44], where references are provided for the simulations data shown).

heating, such as foil disassembly under the thermal pressure of hot electrons, or debunching of the compressed foil [39], and to dominate over TNSA. For this purpose, simulations have mostly used circularly polarized (CP) pulses, for which the ponderomotive force does not oscillate within a cycle, and electron heating mechanisms such as $J \times B$ heating are in principle suppressed [40]. Recent work has, however, highlighted hybrid RPA-TNSA regimes using linearly polarized pulses, where, under appropriate conditions, RPA features dominate the ion spectra [41], and has investigated the more complex dynamics associated with RPA of multispecies targets.

Experiments employing ultrathin foils have recently started to show signatures of RPA acceleration processes, namely effective acceleration of bulk species [42], spectral peaks [43–45], fast scaling consistent with LS theoretical predictions [43]. Fig. 3 shows experimental data from [43] plotted against data from published 2D PIC simulation, and scaling from a simple LS model. The steep rise in ion energy obtainable by either decreasing the areal density or increasing the fluence is extremely encouraging. For example, starting from the experimental data, taken using 100 nm Cu irradiated at 3×10^{20} W/cm^2, one may be able to reach 100 MeV/nucleon energies by increasing the fluence by a factor 2 and decreasing the target density by a factor 2.5 [43].

5.4. Relativistic transparency regimes

Acceleration regimes in which the target becomes relativistically transparent to the laser pulse are also of interest, and have been explored recently in a number of experiments [46–49]. In these investigations the target areal density is chosen so that the target is quickly heated by the laser pulse, and the density decreases below the relativistically corrected critical density near the peak of the pulse. In this regime the interaction leads to volumetric heating of the target electrons, and to a consequent enhancement of the field accelerating the ions. In the *Break Out Afterburner* scenario proposed by the Los Alamos group [50], nonlinear processes lead to growth of electromagnetic instabilities, which further enhances energy coupling into the ions.

Experimental spectra obtained in this regime are generally broadband, with particle numbers decreasing to a high energy plateau and show efficient acceleration of the bulk components of the target. Cut-off energies for C^{6+} ions from DLC target ranging from 40 Mev/nucleon [47] to a record 80 MeV/nucleon [49] have been recently inferred from experimental data. This latter result employed target cleaning techniques to remove the proton contaminants and increase the efficiency of the acceleration of the bulk species.

Deuteron ions produced in this regime of acceleration have recently been used to drive, with high efficiency, neutron production from nuclear reactions initiated in a secondary Be target [51].

Acknowledgments

The author acknowledges support from EPSRC Grant EP/K022415/1 and from Projects ELI (Grant no. CZ.1.05/1.1.00/483/02.0061) and OPVK 3 (Grant no. CZ.1.07/2.3.00/20.0279), and discussions with/contributions from A. Macchi, M. Passoni, J. Fuchs, D. Jung, D. Margarone, K. Prise, G. Schettino, P. McKenna and Z. Najmudin.

References

[1] E.L. Clark, et al., Physical Review Letters 84 (2000) 670.
[2] A. Maksimchuk, et al., Physical Review Letters 84 (2000) 4108.
[3] R.A. Snavely, et al., Physical Review Letters 85 (2000) 2945.
[4] S.C. Wilks, et al., Physics of Plasmas 8 (2001) 542.
[5] P. Mora, Physical Review Letters 90 (2003) 185002.
[6] M. Borghesi, et al., Fusion Science Technology 49 (2006) 412.
[7] H. Daido, M. Nishiuchi, A.S. Pirozkhov, Reports on Progress in Physics 75 (2012) 056401.
[8] A. Macchi, M. Borghesi, M. Passoni, Reviews of Modern Physics 85 (2013) (751 and references within).
[9] W.L. Kruer, K. Estabrook, Physics of Fluids 28 (1985) 430.
[10] A.J. Mackinnon, et al., Physical Review Letters 88 (2002) 215006.
[11] T. Ceccotti, et al., Physical Review Letters 99 (2007) 185002.
[12] M. Hegelich, et al., Physical Review Letters 89 (2002) 085002.
[13] M. Borghesi, et al., Plasma Physics and Controlled Fusion 50 (2008) 124040.
[14] K. Ogura, et al., Optics Letters 37 (2012) 2868.
[15] K. Zeil, et al., New Journal of Physics 12 (2010) 045015.
[16] K.A. Flippo, et al., Review of Scientific Instruments 79 (2008) 10E534.
[17] A. Macchi, et al., Plasma Physics and Controlled Fusion 55 (2013) 124020.
[18] T. Cowan, et al., Physical Review Letters 92 (2012) 204801.
[19] D. Doria, et al., AIP Advances 2 (2012) 011209.
[20] J. Bin, et al., Applied Physics Letters 101 (2012) 243701.
[21] J. Fuchs, et al., Nature Physics 2 (2006) 48.
[22] L. Robson, et al., Nature Physics 3 (2007) 58.
[23] P. Mora, Physical Review E 72 (2005) 056401.
[24] M. Passoni, M. Lontano, Physical Review Letters 101 (2008) 115001.
[25] M. Passoni, L. Bertagna, A. Zani, New Journal of Physics 12 (2010) 045012.
[26] S. Buffechoux, et al., Physical Review Letters 105 (2010) 015005.
[27] S. Gaillard, et al., Physics of Plasmas 18 (2011) 056710.
[28] D. Margarone, et al., Physical Review Letters 109 (2012) 234801.
[29] S.C. Wilks, W.L. Kruer, M. Tabak, B. Langdon, Physical Review Letters 69 (1992) 1383.
[30] A.P.L. Robinson, et al., Plasma Physics and Controlled Fusion 51 (2009) 024004.
[31] C. Palmer, et al., Physical Review Letters 106 (2011) 014801.
[32] A.P.L. Robinson, R M G M Trines, N.P. Dover, Z. Najmudin, Plasma Physics and Controlled Fusion 54 (2012) 115001.
[33] L. Silva, et al., Physical Review Letters 9 (2004) 015002.
[34] D. Haberberger, et al., Nature Physics 8 (2012) 95.
[35] T. Esirkepov, et al., Physical Review Letters 92 (2004) 175003.
[36] A.P.L. Robinson, et al., New Journal of Physics 10 (2008) 013021.
[37] A. Macchi, S. Veghini, F. Pegoraro, Physical Review Letters 103 (2009) 085003.
[38] B. Qiao, et al., Plasma Physics and Controlled Fusion 53 (2011) 124009.
[39] B. Qiao, et al., Physical Review Letters 102 (2009) 145002.
[40] A. Macchi, et al., Physical Review Letters 94 (2005) 165003.
[41] B. Qiao, et al., Physical Review Letters 108 (2012) 115002.
[42] A. Henig, et al., Physical Review Letters 103 (2009) 245003.
[43] S. Kar, et al., Physical Review Letters 109 (2012) 185006.
[44] S. Steinke, et al., Physical Review Special Topics – Accelerators and Beams 16 (2013) 011303.
[45] B. Aurand, et al., New Journal of Physics 15 (2013) 033031.
[46] A. Henig, et al., Physical Review Letters 103 (2009) 045002.
[47] B. Hegelich, et al., Nuclear Fusion 51 (2011) 083011.
[48] D. Jung, et al., New Journal of Physics 15 (2013) 023007.
[49] D. Jung, et al., Physics of Plasmas 20 (2013) 083103.
[50] L. Yin, et al., Physical Review Letters 107 (2011) 045003.
[51] M. Roth, et al., Physical Review Letters 110 (2013) 044802.